DEVELOP Technical Report

Davidson Health & Air Quality II

Assessing Urban Heat and Tree Canopy to Inform Urban Planning in Davidson, North Carolina

Summer 2025 | Virginia – Langley
August 8th, 2025

Authors: Ava Johnson (Analytical Mechanics Associates), Isaac Xie (Analytical Mechanics Associates), Jimmy Stephens (Analytical Mechanics Associates), Julian Alcantara (Analytical Mechanics Associates)

Abstract: The Town of Davidson, North Carolina strives to make their community more sustainable through the implementation of a robust Climate Action Plan (CAP). The CAP included goals to improve the local ecosystem through a comprehensive urban forestry plan and enhancing Davidson's resilience to urban heat. However, from examining land imagery, many wooded areas have been cut down to make way for constructing new developments from 2015 to 2025. Davidson staff previously lacked the resources to assess tree canopy coverage and other factors affecting local temperatures, so therefore outsourced these tasks to private companies. The DEVELOP team analyzed observations from Landsat 8 Operational Land Imager (OLI) and Thermal Infrared Sensor (TIRS), Landsat 9 OLI-2 and TIRS-2, and International Space Station's ECOsystem Spaceborne Thermal Radiometer Experiment on Space Station to investigate how urbanization has affected the community's environment and contributed to changes in the local climate. Maps created using these observations highlighted changes in tree canopy, vegetation health, and urban heat. Further analysis of the area incorporating aerial imagery and social vulnerability data aided in identifying locations most vulnerable to heat. Davidson staff can use our results to conduct their own in-house analyses and focus their heat mitigation efforts where they are most needed.

Key Terms: remote sensing, urban heat island, tree canopy, albedo, Landsat, ECOSTRESS

Advisors: Dr. Xia Cai (NASA Langley Research Center), Dr. Kenton Ross (NASA Langley Research Center), David Young (NASA Langley Research Center)

Lead: Jack Graziano (Virginia – Langley)

Previous Contributors: Briana Johnson, Drew Emerine, Samatha Ziemba, Tanya Kasyanchuk

1. Introduction

Extreme heat can have severe consequences for public health. According to the World Health Organization, heat events can exacerbate existing health conditions, facilitate the spread of vector-borne diseases, and result in socioeconomic damage. Excessive heat is especially dangerous to our most vulnerable populations, such as the elderly, pregnant, homeless, and ill. Furthermore, considering the implications of climate change across the globe, the impacts of extreme heat have become a major concern. Worldwide, there are approximately 489,075 heat-related deaths per year (Zhao et al, 2021). In the years between 2000-2004 and 2017-2021, there was an 85% increase in heat-related deaths for people aged 65 and older (World Health Organization, 2024).

Large cities typically lack ample tree canopy coverage and contain an abundance of low-albedo pavements and high density of buildings, which are conducive to increased temperatures (Cheela et al., 2021; Loughner et al., 2012). This phenomenon in which more urbanized areas experience higher temperatures is known as the urban heat island (UHI) effect. Analysis of these aspects that contribute to UHIs may be used to implement proper risk management, smart urban planning, and preparation to mitigate associated adverse health effects.

Remote sensing offers ideal methods and technologies to accurately assess the effects of UHI and associated mitigation efforts at community scale. Researchers have utilized Earth observations (EOs) to measure land surface temperatures (LST) and map regional and global heat waves (Hu et al., 2023). LST provides information about the surface's captured thermal emissions and surface energy budget, making it instrumental in monitoring urban heat. Landsat 8's Thermal Infrared Sensor (TIRS) detects the energy radiated from the Earth's surface, making it especially useful in calculating LST (Zargari et al., 2024). Landsat 8 also provides high-resolution imagery from its Operational Land Imager (OLI), capable of detecting the visible and infrared spectrum. Landsat OLI data can be used to calculate normalized difference vegetation index (NDVI), a metric for determining vegetation health and measuring tree canopy coverage (D'Allestro & Parente, 2015). NDVI data is crucial to assessing UHI effects, as maintaining tree canopy is extremely efficient in mitigating urban heat. Furthermore, Chen et al. (2006) found that vegetation distribution and density can even combat increasing temperatures by analyzing LST and NDVI.

Partnering with the Town of Davidson, we aimed to assess the feasibility of mapping urban heat and canopy coverage by using NASA EOs. Our team conducted a heat "hot spot" analysis of the study area which can aid in identifying areas for green infrastructure to reduce the UHI effect. This was the second DEVELOP project working with the Town of Davidson. The first project team provided the Town of Davidson—and former partner, cleanAIRE NC—with concentration maps of gaseous pollutants including NO_2 and particulate matter (PM), bivariate maps combining levels of gaseous pollutants and social vulnerability index, and time-series correlation plots on satellite observations and ground measurements. These maps were beneficial to locating the highest levels of particulate matter and NO_2 in the study area. When the first project concluded, the team found a slightly positive relationship between PM concentration and proximity to highways. The results also suggested a minor correlation between asthma rates and levels of air pollutants.

The study area for this project focuses on the Town of Davidson, including the surrounding Charlotte Metropolitan area (Figure 1). Within these limits, a vegetated reference area consisting of about 100.0 acres of forestry was established to compare temperatures to urbanized locations (Figure E1). The study period was from January 2015 to May 2025, as Davidson's 46% population increase during those years is especially applicable for studying social vulnerability and urban growth (Macrotrends, 2025). Davidson is committed to making their town more sustainable, as delineated in their Climate Action Plan (CAP). To support the development of a more sustainable community, the CAP calls for developing an Urban Community Forestry Plan guided by previously conducted tree canopy inventories and associated canopy assessments (Town of Davidson, 2024). Integrating GIS techniques to analyze environmental planning outcomes can further strengthen Davidson's CAP to be a model for other small towns to take inspiration from in their own environmental planning.

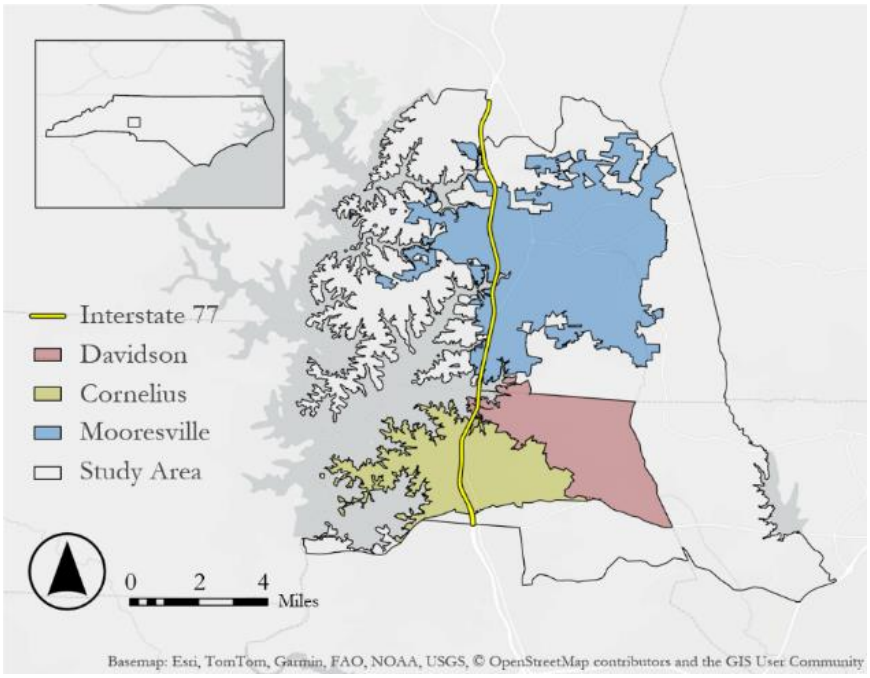

Figure 1. Map of Davidson, North Carolina and surrounding study area

2. Methodology

This study utilized a variety of satellites, sensors, ancillary datasets, and remote-sensing techniques in order to address the Town of Davidson's concerns regarding urban heat. We used data from Landsat OLI and TIRS, Landsat 9's OLI-2 and TIRS-2, The International Space Station's ECOsystem Spaceborne Thermal Radiometer Experiment on Space Station (ECOSTRESS), the National Agriculture Imagery Program (NAIP) and the 2022 Social Vulnerability Index (SVI) (Table B1). The study consisted of three main steps in which data were acquired, processed, and analyzed in order to map the urban heat trends of our study area. We generated maps of urban heat islands, albedo, vegetation health, social vulnerability, and finally a hot spot analysis looking at heat exacerbating and mitigating factors which our partners can use to aid their plans in sustainable development.

2.1 Data Acquisition

2.1.1 Urban Heat, Albedo and Vegetation

To assess the urban heat, albedo, and vegetation health of our study area, we used Collection 2 Level 2 data from the Landsat 8 OLI and TIRS and Landsat 9 OLI-2/TIRS-2 (Earth Resources Observation and Science, 2020). We accessed these data through the United States Geological Survey (USGS) Earth Explorer tool, specifying our study area with a polygon and using the temporal ranges of 2015-2020 and 2023-2025. The launch of Landsat 9 in 2021 allowed for a smaller temporal range in our present-day analysis due to an increase in data. To limit cloud contamination, scenes were filtered within to contain a maximum cloud coverage of 20% prior to downloading the data.

2.1.2 Evapotranspiration and Nighttime LST

To evaluate evapotranspiration (ET), we used Collection 2 Level 3 Tiled (L3T) data from ECOSTRESS onboard the ISS. The data were downloaded from NASA Earthdata Search and filtered by temporal range for each year and the geographical range of our study area. A similar process was used to download Level 2 Version 2 Tiled (ECO_L2T_LSTE) scenes and quality control layers for LST, which was atmospherically corrected prior to collection. Since ECOSTRESS was launched on July 29, 2018, we began collecting 70-meter resolution data ranging from August 2018 to July 2025. The data were available for all years except 2022 due to a glitch in the correction code but is estimated to be released in August 2025.

2.1.3 Tree Canopy Coverage

Optical imagery from NAIP data (USDA NAIP Geohub) was used for tree canopy land classification. The NAIP imagery was downloaded from the USGS Earth Explorer for 2016 (1-m resolution) and 2022 (0.6-m resolution), with images in May, June, and September of both years. To procure needed NAIP imagery, a study area on Earth Explorer was made to surround the project shapefile, and the resulting images were cross-checked manually to encompass the shapefile on ArcGIS Pro. Subsequently, the NAIP data were uploaded for both 2016 and 2022 onto ArcGIS Pro for processing.

2.1.4 Heat Vulnerability

To assess heat vulnerability, we utilized local temperatures and social vulnerability data. We acquired LST data from June 2024 to May 2025 using the same methods mentioned in section 2.1.1. The 2022 Social Vulnerability Index (SVI) – published by the CDC and Agency for Toxic Substances and Disease Registry (ATSDR) through their Geospatial Research, Analysis, and Services Program (GRASP) – was used for the social component of this analysis (CDC & ATSDR, 2024). The SVI evaluates populations' social vulnerability by analyzing various social aspects falling under four themes: socioeconomic status, household characteristics, racial and ethnic minority status, and housing type and transportation as seen in Figure A1. GRASP released these data as a comma-separated values (CSV) file that we downloaded at the census-tract level for processing.

2.1.5 Projected Near-Surface Air Temperatures

In addition to data trends and present-day analysis, the Town of Davidson was also interested in future temperature predictions for our study area. Using Google Earth Engine (1.6.2rc0), the team was able to extract projected atmospheric temperature data from NASA's NEX-DCP30 climate prediction models at 30 arcsecond latitude resolution (~ 1km at the Equator and finer at higher latitude). Since atmospheric temperature is usually measured at 2 m above the ground it is lower than the LST, however it shows a similar trend. We selected three different US-based models: Coupled Model-3 from the Geophysical Fluid Dynamics Laboratory (GFDL-CM3), Community Earth System Model version 1.0 with Community Atmospheric Model version 5 (CESM1-CAM5) from the National Center for Atmospheric Research, and ModelE2 version of NASA Goddard Institute for Space Studies General Circulation Model (GISS-E2-R). We chose Representative Concentration Pathway (RCP) 4.5 which is a scenario that stabilizes radiative forcing at 4.5 Watts per meter squared for each model. To compare the maps in temperature between models, we collected the maximum monthly atmospheric temperature for each of the two 10-year timeframes of 2020-2030 and 2045-2055. We also collected time series data between the years of 2025-2050 for each model. The data were then saved as CSV files for further analysis.

2.2 Data Processing

2.2.1 Urban Heat

Using a Python script written in Visual Studio Code (1.102.0), we first filtered the Landsat scenes for clear imagery and sufficient data coverage over our study area. From each infrared scene, our Python script selected the thermal infrared band 10 (Band 10) with wavelengths between 10.6 and 11.19 micrometers and the associated Pixel Quality Assessment (QA_Pixel) band. These bands are used to retrieve the LST and to denote image quality, respectively. Images were clipped to our study area shapefile to ensure valid data coverage over our area of interest and to reduce processing times. The QA band was decoded utilizing a bitwise interpretation and then used to mask each image for clouds, shadows, or poor-quality pixels, using a medium cloud confidence threshold. Images were then rescaled using the scale factor and offset as provided by USGS (2023) before being converted from Kelvin to Fahrenheit for increased accessibility to our partners (Equation 1).

$$T_K = T_{pixel} \times 0.00341802 + 149.0 \quad (1)$$

Finally, we filtered the images to keep only those with a minimum of 50% valid pixels over the study area. This process yielded 35 usable images for both 2015-2020 and 2023-2025.

2.2.2 Albedo and Vegetation

To filter and process the data for albedo and vegetation, we used a modified version of the script used to process LST data. We clipped, masked, and filtered Landsat 8 OLI and Landsat 9 OLI-2 reflectance scenes using the same process as above. A different USGS rescaling and offset was applied to convert digital number of pixel (DN) of visible and near-infrared bands (bands 1-7) to surface reflectance (SR) (Equation 2).

$$SR = DN \times 0.0000275 - 0.2 \quad (2)$$

Images that did not meet the minimum data coverage of 50% were rejected, and valid images were saved for further analysis.

2.2.3 Evapotranspiration (ET) and Nighttime LST

To process the acquired ET and nighttime LST data, we wrote three Python scripts in visual studio code. First, Level 2 Nighttime LST images were masked using the associated quality control layers in the first script. The second script loaded the data, applied a clipping function, filtered based on valid pixel percentage (≥50%), and saved the remaining GeoTIFF images. The third script categorized the valid images into separate time intervals, 2018-2020 (before) and 2021-2025 (after), as well as seasons, summer and winter. Sorting by season was necessary due to an uneven seasonal distribution for ECOSTRESS data when looking at the entire temporal range.

2.2.4 Tree Canopy Coverage

We used the merge rasters function in ArcGIS Pro to create two continuous mosaics—one for 2016 and one for 2022—for further analysis. Then, we performed land classification using the Classification Wizard tool on both the 2016 and 2022 NAIP mosaics. Each classification was supervised with the following classes: water, developed, barren, forest, herbaceous, and plant/cultivated. Five to seven samples were identified for each class to train the program using the K-Nearest Neighbor classifier, which then sorted the remaining pixels for each mosaic into a class. To distinguish the tree canopy areas of each mosaic, we applied a reclassification, merging the non-forest classes to create a binary forest and non-forest mosaic for both years.

2.2.5 Heat Vulnerability

Prior to analyzing for heat vulnerability, LST and SVI were established for each census tract of the study area. We used the Zonal Statistics tool in ArcGIS Pro on the LST composite raster to calculate the median temperature for each tract, then classified them into three rankings, i.e., 77-83 °F, 83-88 °F, and 88-94°F to mark communities experiencing low, medium, and high LST. To compare these classes to social vulnerability factors, we uploaded the SVI CSV into Microsoft Excel to filter it to the census tracts in our study area and select the appropriate variables to assess heat vulnerability. We selected 13 SVI percentage variables such as people without health insurance, people aged 65 years and older, and housing structures with 10 or more units (all are detailed in Table A1). Once we had established the social vulnerability variables, the percentages for each tract were averaged and divided into three classes, i.e., 2-5%, 5-10%, and 10-15% to represent communities with low, medium, and high social vulnerability. Filtering and classifying both datasets prepared them for heat vulnerability analysis.

2.2.6 Projected Temperatures

To complement the projected temperature CSV tables, we also produced mean composite GeoTIFF images from the three selected atmosphere models in Google Earth Engine. We used summer months (June, July, August) for each timeframe to visualize the atmospheric temperature pattern across our study area. For each model, we generated one image per timeframe, yielding a total of six images which were then saved for further analysis.

2.3 Data Analysis

2.3.1 Urban Heat

To calculate UHI, we established a reference area filled with dense, healthy trees just to the east of Davidson to compare to the rest of the study area. The team wrote a Python script that subtracted the median LST of our wooded reference area from the study area values for each filtered, valid image in each timeframe (Equation 3). This index visualizes the differences in temperatures between urban areas and reference area. After calculations, the resulting images were then composited to create a time series map to showcase the differences in urban heat between the years of 2015 and 2025. We aggregated 35 valid images each from the years of 2015-2020 and the years of 2023-2025 to create two median composites. To visualize the change in urban heat, we subtracted the temperature values of the 2015-2020 composite from those of the 2023-2025 composite using the raster calculator tool in ArcGIS Pro (3.5.0).

$$UHI = T_{Study\ Area} - T_{Reference\ Area} \tag{3}$$

2.3.2 Albedo

To estimate the surface albedo (α) of our study area, we used the V03 method (Equation 4, Andres-Anaya et al., 2023) for the valid images in each timeframe. In this equation, ρ_λ is the monochromatic reflectance of the spectral band λ as specified for Landsat 8 in Table 1. For this feasibility study, we assumed that Equation 4 could be applied to Landsat 9 OLI-2 data given the similarity of OLI and OLI-2. Applying the formula created an index, α, from 0-1, with 0 representing low albedo surfaces that absorb the most light, and 1 representing high albedo surfaces that reflect the most light. Following the same methods as our UHI yearly aggregates, the images were then used to create two median composites for the years of 2015-2020 and 2023-2025. Finally, we created a time series map visualizing the change in albedo over our study period.

$$\alpha = 0.043 + 0.082 \cdot \rho_1 + 0.064 \cdot \rho_2 + 0.173 \cdot \rho_3 + 0.114 \cdot \rho_4 + 0.237 \cdot \rho_5 + 0.252 \cdot \rho_6 + 0.034 \cdot \rho_7 \tag{4}$$

Table 1

Reflectance bands of the Landsat 8 OLI sensor used in the computation of surface albedo (Andres-Anaya et al., 2023)

Bands	**Wavelength (μm)**
Band 1–Coastal Aerosol	0.43–0.45
Band 2–Blue	0.45–0.51
Band 3–Green	0.53–0.59
Band 4–Red	0.64–0.67
Band 5–Near Infrared (NIR)	0.85–0.88
Band 6–Short-wave Infrared (SWIR) 1	1.57–1.65
Band 7–Short-wave Infrared (SWIR) 2	2.11–2.29

2.3.3 Vegetation

To assess the vegetation health of our study area, we calculated the NDVI for each time frame. For each reflectance scene, we used surface reflectance of red and near infrared (NIR) bands (Band 4 and 5) from Landsat 8 OLI and Landsat 9 OLI-2. The team wrote a Python script that processed each filtered, valid image using the selected band pairs and the NDVI equation (Equation 5, Kriegler et al., 1969). The results produced an index from -1 to 1, with 1 representing the most dense, healthy vegetation and -1 representing none. We aggregated the images for each timeframe into two median composites, then subtracted to create a map showcasing the change in NDVI.

$$NDVI = \frac{(NIR - Red)}{(NIR + Red)} \tag{5}$$

2.3.4 ET and Nighttime LST

After processing, valid ECOSTRESS images were aggregated to create median composites of ET and nighttime LST for each time frame using a Python script. We created four composites of evapotranspiration, consisting of a summer and a winter seasonal aggregate for each time frame. Due to limited summer images of nighttime LST, only two yearly aggregates were produced for 2018-2021 and 2022-2025. Finally, in ArcGIS Pro, the Project Raster tool was used to accurately align the composite images to the proper XY coordinates, WGS 1984.

2.3.5 Tree Canopy Coverage

We evaluated the accuracy of the tree canopy binaries using 200 stratified random pixels on both of the mosaics. Each point was manually ground-truthed in ArcGIS Pro to determine if the classification accurately labeled the pixel as a "tree" or "not tree." The results of the manual accuracy process are presented in Table 1 and Table 2.

Table 2

Confusion Matrix of tree canopy classification using 2016 NAIP observations

		Reference Data			
Classified Data	2016 Binary	**Tree**	**Not Tree**	**Total**	**User's Accuracy**
	Pixel Tree	74	10 (false positive)	84	88.1%
	Pixel Not Tree	28 (false negative)	88	116	75.9%
	Total	102	98	200	
	Producer's Accuracy	72.5%	89.8%		81.0%

The 2016 confusion matrix returned producer's accuracy i.e. recall: how well a specific class was classified by the model, values of 72.5% for tree pixels and 89.8% for non-tree pixels. The user's accuracy i.e. precision: how likely the classification was correct, values were 88.1% for tree pixels and 75.9% for non-tree pixels. The process yielded an overall accuracy of 81.0%. The Cohen's Kappa value is 0.621. The standard error (SE) of 0.054, 95% confidence interval is [0.515, 0.728], indicating a high level of agreement, or low likelihood that the overall accuracy would be substantially lower than our results.

Table 3

Confusion Matrix of tree canopy classification using 2022 NAIP observations

		Reference Data			
Classified Data	2022 Binary	**Tree**	**Not Tree**	**Total**	**User's Accuracy**
	Pixel Tree	64	3 (false positive)	67	95.5%
	Pixel Not Tree	25 (false negative)	108	133	81.2%
	Total	89	111	200	
	Producer's Accuracy	71.9%	97.2%		86.0%

The 2022 confusion matrix yielded producer's accuracy values of 71.9% for trees and 97.2% for non-trees. The user's accuracy values were 95.5% and 81.2% for trees and non-trees, respectively. The overall accuracy of the 2022 land classification was 86%. The Cohen's Kappa value is 0.709 (SE of 0.050, 95% CI of [0.612, 0.807]), indicating a high level of agreement, or low likelihood that the overall accuracy would be substantially

lower than 0.86, e.g. 0.7. In both confusion matrices, the overall accuracy rate was deemed acceptable at a 75% rate or above which both exceeded. 75% was the team's target accuracy given that the work represented a rapid feasibility assessment. Thus, the land classifications were considered sufficiently accurate.

To produce a tree canopy change map, we utilized the minus function in ArcGIS Pro to subtract the 2016 binary pixels from the 2022 binary pixels. The map displayed areas in which tree canopy has increased, decreased, or did not change between 2016 and 2022. The 2022 binary image was also used as an input for analyzing the area for heat hot spots.

Subsequently, we evaluated the percent change of tree canopy between 2016 and 2022 for the general study area and the town of Davidson. For the general study area, the percent tree canopy in either year was determined based on the number of pixels representing tree canopy and those not, and then the 2016 percent tree canopy was subtracted from the 2022 percent tree canopy to get the change. For the town of Davidson, the pixels representing increase in tree canopy were subtracted from the pixels representing decrease in tree canopy, and then divided by the total number of pixels making up the town.

2.3.6 Heat Vulnerability

The average SVI percentages for each census tract were compared to the median LST to analyze the population's heat vulnerability. These datasets were used to create a bivariate map of the study area, ranking each tract from low to high for both variables. This map served as a visual qualitative analysis to identify which census tracts were most vulnerable to heat.

2.3.7 Heat Hot Spot Analysis

To calculate the Heat Hot Spot (HHS) analysis map, the team used the median NDVI and albedo composites from the years of 2023-2025 combined with the 2022 tree canopy layer. Using the Raster Calculator in ArcGIS Pro, each layer was first normalized using the minimum and maximum values to create an index from 0-1 (Equation 6). Layers were then added together into one map (Equation 7). This created a new index from 0-3, with higher values indicating areas where heat is mitigated, and lower values indicating areas where heat is exacerbated.

$$x = \frac{(x - x_{min})}{(x_{max} - x_{min})} \tag{6}$$

$$HHS = NDVI + Tree\ Canopy + Albedo \tag{7}$$

2.3.8 Projected Temperatures

We imported the CSV files of projected temperature data into Microsoft Excel to generate charts for each model and timeframe. Data were then converted from Kelvin to Fahrenheit for better accessibility. We calculated trendlines and statistics to further understand the temperature trends and the differences in outputs between models. Finally, we averaged the results of all three models together to create a 2025-2050 time series chart. Next, we imported our GeoTIFF images for each model into ArcGIS Pro and converted them to Fahrenheit for consistency. For each timeframe, we averaged the composites for each model into one image, producing two final temperature prediction images.

3. Results

3.1 Analysis of Results

3.1.1 Urban Heat

The hottest areas on the UHI maps included urban and residential areas, parking lots, and construction sites. Throughout the years of 2015 and 2025, the median temperature differences between urban and rural areas were 3.86 and 4.81°F, respectively. Due to increasing population and development in our study area, we were also interested in the changes in UHI patterns throughout the study period (Figure D1). Across the entire

study area, we found a small overall increase in UHI, with the temperature difference increasing by a median of 0.95°F. The histogram revealed that data were skewed to the left, with most of the area experiencing little change, while a smaller proportion of developing spots experienced a notable increase (Figure F1). We set a high UHI change threshold of 2 standard deviations above the mean (4.89°F) and found that 4.03% of the study area experienced a change at or above the threshold, with a maximum up to nearly 20°F higher. Due to limited Landsat and ECOSTRESS data, we utilized images from the entire year, assuming that the same regions would experience the UHI effect regardless of season. To test this hypothesis, we also aggregated images using the months of June, July and August for our two timeframes and created another change map of summer UHI for comparison (Figure D2). We found that the same spatial patterns of relatively hotter and cooler areas were highlighted. Similarly, there was a slight increase in the median temperature difference of the summer UHI from 6.09°F to 7.28°F or higher.

We also generated Nighttime LST maps to complement the daytime UHI analysis. By examining nighttime LST, we identified areas that retain heat throughout the night and pose concerns for heat-related illness. Despite the uneven seasonal distribution of ECOSTRESS data, we discovered that the hottest areas at night were located along the lakes, indicative of water's heat retaining properties (Figure D3).

3.1.2. Vegetation

By calculating the change in NDVI throughout the decade, we were able to identify new areas of development due to their drops in NDVI (Figure D4). Decreases in NDVI were generally consistent with increases in UHI. Some areas experienced vegetation growth, most notably a tree farm near the center of Davidson. Across the entire study area, there was a small overall decrease in NDVI with a median difference of -0.03. The histogram of NDVI change data mirrored that of UHI, in which the data were skewed to the right (Figure F2). Most of the area experienced little change, though there was a small proportion that experienced notable decreases in NDVI. About 4.17% of the study area experienced a decrease in NDVI of at least 2 standard deviations below the mean (-0.25), which we identified as sites of human activity.

3.1.3 Albedo

Upon analyzing the albedo change map (Figure D5), we noticed that areas of development generally experienced increases in albedo. This is most likely due to removal of vegetation–which is very absorptive and photosynthesizes energy rather than storing it as heat–and replacing it with bare soil, construction materials, or white-roofed buildings. Even though high-albedo surfaces do have some effect in reflecting energy and reducing the UHI effect, they are not nearly as efficient as tree canopy coverage. Many areas of increased albedo also experienced an increase in UHI as a result of the vegetation loss mentioned above. The histogram was extremely left-skewed (Figure F3), with the entire study area experiencing a median decrease in albedo of about 0.49%. However, about 2.52% of the study area experienced a notable increase in albedo of about 4% or greater.

3.1.4 Evapotranspiration

Following a review of the four ET maps, only the 2018-2020 summer map was usable due to its quality. Based on the map (Figure E6), we observed that the area to the east of Interstate 77 had significantly higher ET rates compared to the western side. This observation can be supported by the fact that the region described is mostly forested land. The evapotranspiration values in the forested areas reached as high as 5 mm/day, while the lowest recorded was 0.7 mm/day in urban areas. This comparison highlights the role of tree canopy cover in enhancing evapotranspiration.

3.1.5 Tree Canopy Coverage

We found that tree canopy coverage decreased overall in both the general study area (-7.7%) and in the town of Davidson (-14.1%), as seen in Figure D6. These decreases coincide with the increase in urbanization in Davidson and surrounding areas between 2016 and 2022. There were also notable canopy increases in downtown Davidson, where policy supporting tree planting (Davidson Lands Conservancy) was implemented in the study period. Additionally, tree canopy increases also highlighted development of some tree farms. By

focusing analysis on certain neighborhoods, such as a set of neighborhoods adjacent to each other in southern Davidson, our observations support tree canopy as more effective than albedo increase. The newer neighborhood to the west, which was developed sometime between 2016 and 2022 (Figure E2), experienced a decrease in canopy and increase in albedo, which contributed to the increase in heat. The adjacent neighborhood, which largely stayed the same although may have increased tree canopy slightly, became slightly cooler.

3.1.6 Heat Vulnerability

The comparison of census tract SVI and median LST revealed that areas most vulnerable to heat largely coincided with those of reduced tree canopy cover and increased urbanization (Figure 2). The least vulnerable tracts largely included forested and rural regions to the east of the study area, as well as high-income neighborhoods with pronounced tree canopy on the shores of Lake Norman. Downtown Mooresville and Cornelius, as well as other locations along Interstate 77, experienced the highest LST and social vulnerability, likely due to increased traffic through these areas and their more developed environments. Primary SVI factors contributing to the heat vulnerability include (in order of importance) "population spending 30% or more of their income on housing", "population being 65 years or older", and "housing structures containing 10 or more units". The Town of Davidson exhibited these factors as well, which could be due in part to the student population at Davidson College and multiple retirement communities in the town. The most heat vulnerable census tract in Davidson borders Cornelius on the shore of Lake Norman. This area encompasses the town's central business district, a retirement community, and several apartment complexes and other residences. These heat vulnerability findings, in conjunction with the hot spot analysis, aided in identifying potential locations to focus heat mitigation efforts.

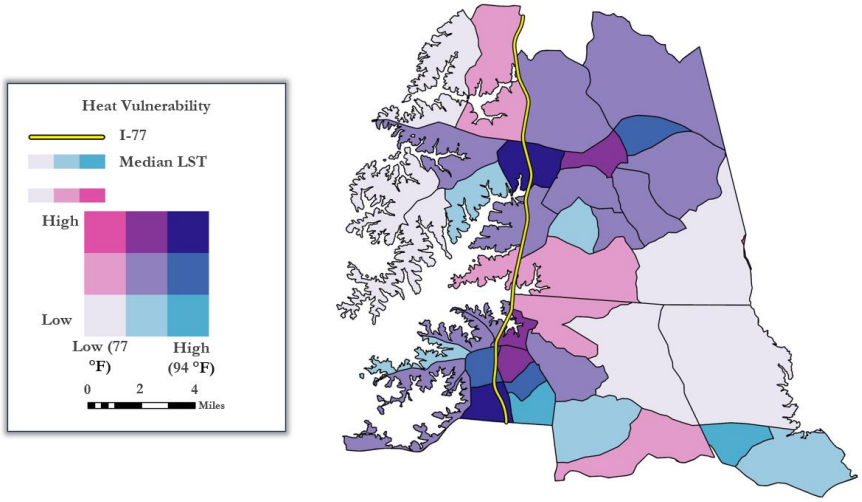

Figure 2. Heat vulnerability map distinguishing between census tracts less vulnerable to heat in lighter colors and those that are more vulnerable to heat in darker colors

3.1.7 Heat Hot Spot Analysis

The HHS analysis map revealed areas that mitigate heat most efficiently and those that are most exacerbating (Figure 3). In general, areas that held the most heat mitigating potential had significant tree canopy coverage and a high NDVI value, even if albedo was low, since the higher absorption refers to vegetation in these cases. Areas of moderate heat mitigation tended to be open fields, farmlands, or buildings with white roofs. This indicates that although canopy coverage is most efficient in mitigating heat, implementing reflective surfaces does have a cooling effect when compared to dark surfaces. The most heat-exacerbating areas included dense urban sites, neighborhoods, and parking lots with little vegetation and dark, highly absorptive surfaces. Overlaps between the HHS analysis map and UHI maps validated the hot spot analysis.

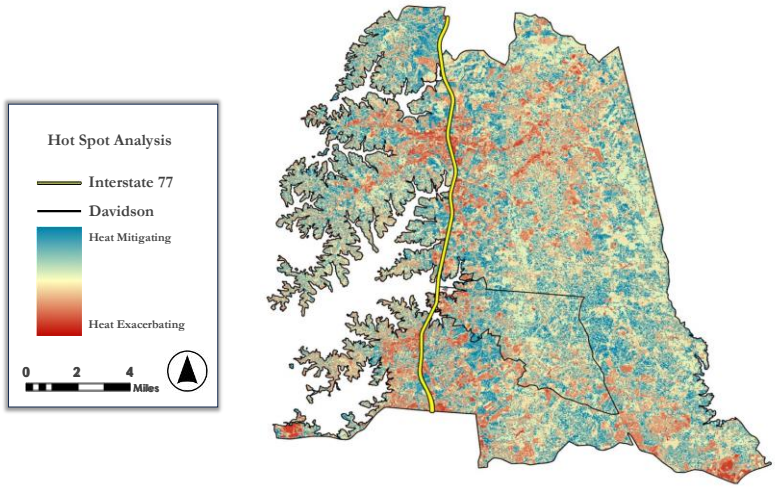

Figure 3. HHS Analysis Map

3.1.8 Projected Temperatures

All three models predicted a small increase in atmospheric temperature between our two timeframes of 2020-2030 and 2045-2055, with an average of 1.44°F higher across the entire study area. The predicted increase was similar for the summer months, with the study area expecting atmospheric temperatures to be about 1.50°F higher. The time series chart predicted a steady increase in atmospheric temperatures from 2025 until 2038, when there was a sudden drop before steadily climbing again (Figure F4). Even though air temperature is different from LST and does not consider influence of surface type such as soil, asphalt, or water, it can still be a useful estimation of temperature trends.

3.2 Errors & Uncertainties

3.2.1 Urban Heat

The results of the urban heat analysis were limited to the availability of cloud-free satellite images. Many LST images featured anomalies in the northeast corner of our study area, with several pixels missing or holding extreme temperature values. Although we used median values in our composites to combat this, there is still a potential for error.

To attain enough images to generate a usable composite, we had to create a time frame spanning multiple years for both the past and present analysis. This posed the risk of an uneven seasonal distribution of images (Figure C1), which would skew the temperatures of the final composite to appear artificially hotter or cooler. The ECOSTRESS data were especially affected by seasonal skewness, as very few usable summer images generated composites biased towards cooler months (Figure C2).

Additionally, differences in satellite resolution also limited the urban heat analysis. Although Landsat's TIRS data are rescaled to a 30m resolution to be consistent with OLI, the true resolution is 100m. Additionally, ECOSTRESS data are produced at 70m resolution. Lower-resolution sensors produced coarser maps, making it difficult to identify areas of interest at a more detailed local scale.

3.2.4 Evapotranspiration

The ECOSTRESS data coverage over our study area were limited. Of the 4 maps that we generated, only 1 was considered usable (Figure E6). The remaining maps contained grid-like patterns and long dark marks (Figure E4, E5, and E7). These errors were a direct result of the lack of data that were available when producing the maps. In shown in Table C3, there were only 6 raster images each for the summer and winter seasons of 2018 and 2020. Furthermore, there were 19 and 12 raster images for the summer and winter

throughout the years 2021 to 2025, respectively. The total amount of images per season was not enough to create a high-quality, accurate image. Additionally, in the year 2022, there was no data available due to a processing error which was caused by a glitch in the correction code. The lack of data was consistent for 2021 as well but was luckily released in July 2025. The data for 2022 is estimated to be released in August 2025, unfortunately after the conclusion of this study.

3.2.5 Tree Canopy Coverage

The land classifications introduced error as shown in Table 2 and Table 3, particularly due to the somewhat high false negative rates. These false negative rates were most likely due to the shadows of dense trees classified as "not tree" while darker grass of planted areas may be characterized as tree. This may have led to a portion of the false positive rate. However, the false positive rate was low overall, so this effect does not seem to have been profound. Additionally, the difference in NAIP resolution between 2016 and 2022, with 2022 being higher, may have allowed the overall accuracy rate to be higher in 2022. In the northeast corner of the map, where a seemingly notable tree canopy increase occurred, it is an example of darker grass misclassified as tree.

3.2.6 Heat Vulnerability

Differences in the dates of data used to map heat vulnerability may have introduced uncertainty in this analysis. The CDC published its most recent SVI in 2022, and the composited Landsat data came from 2024 and 2025. While this captures a more recent depiction of the area's temperatures, aspects of social vulnerability may have changed since the release of that data. The SVI may also present uncertainties in its representation of the Town of Davidson, as the town's boundaries do not fully align with those of the census tracts. This could have skewed the analysis of social vulnerability, and subsequently of heat vulnerability, of some portions of the town. Despite these mismatched boundaries, the SVI factors exhibited by the tracts remained the same and offer valuable insights into the residents' vulnerability to heat.

3.2.7 Heat Hot Spot Analysis

Although past projects traditionally used ET data to produce HHS maps, we used NDVI for two main reasons: Landsat's higher resolution of 30m and a lack of reliable ECOSTRESS data over our study area. We found that the map falsely highlighted several small, inland bodies of water as highly heat exacerbating. This is likely due to the tendency of water to score a 0 on all three indexes due to its low albedo, low NDVI, and lack of canopy coverage. Additionally, the accuracy of the HHS map was only as good as the data that went into it. Errors in canopy coverage, for example, would continue to appear in the HHS map.

3.2.8 Projected Temperatures

The results for projected temperatures were based on model outputs and may not be realistic. Yearly projections fluctuated greatly, with some models under- or over-predicting, making it necessary to average the results between timeframes and between models. The coarse 1km resolution made it difficult to analyze data on a small scale. Finally, the models only predicted the atmospheric temperature rather than LST, making it difficult to correlate this data with other factors such as NDVI or albedo.

4. Conclusion

4.1 Interpretation of Results

The Town of Davidson's increased development over the past ten years has made notable impacts on the community's environment. The reduced heat mitigating capacity caused by tree canopy loss and the installation of hard, human-made surfaces that retain heat has paved the way for the formation of UHIs. Despite the rising temperatures, the significant number of trees and light-colored roofs throughout the more urban districts made Davidson's commitment to sustainable urban planning apparent. However, areas with higher temperatures and more vulnerable populations could benefit from the implementation of heat mitigating infrastructure. Williams Place Gracious Retirement Living and other Lakeshore residences experienced the highest temperatures in the most vulnerable area of the town, while the expansive parking lot at the Harry L Vance Athletic Center and the St. Albans neighborhood exhibited the highest LST in all of

Davidson. These locations could benefit from installing more reflective surfaces or vegetated roofs or walls on buildings. Furthermore, several neighborhoods in the town could also benefit from these strategies and planting more trees, as they exhibited increased temperatures over the study period as well. As Davidson's population continues to grow and more urbanization takes place, the town staff can incorporate the analysis of satellite data into their planning to maintain a healthy and sustainable community.

4.2 Feasibility & Partner Implementation

The methodologies delineated in this study can enable our partners at the Town of Davidson to conduct their own efficient, and more cost-effective in-house assessment of tree canopy coverage instead of outsourcing to private contracting companies. These methods also proved that NASA EOs can grant the town's planners the ability to analyze urban heat and other associated factors, such as albedo and social vulnerability. The town's already robust Climate Action Plan did not previously consider the impact that albedo and excessive amounts of exposed pavements can have on local temperatures, but incorporating these considerations could aid in making the community even more sustainable and resilient to heat. The analysis of tree canopy coverage and albedo to identify hot spots of exacerbated UHI effect in the area, as well as recognizing the more vulnerable populations, will narrow their heat mitigation efforts to locations that will most benefit the Town's residents.

5. Acknowledgments

Any opinions, findings, and conclusions or recommendations expressed in this material are those of the author(s) and do not necessarily reflect the views of the National Aeronautics and Space Administration.

This material is based upon work supported by NASA through contract 80LARC23FA024.

Project Partners:

- Town of Davidson

Science Advisors:

- Dr. Xia Cai – Langley Research Center
- Dr. Kenton Ross – Langley Research Center
- David Young – Langley Research Center

Previous DEVELOP Contributors:

- Briana Johnson, Samantha Ziemba, Drew Emerine, & Tanya Kasyanchuk

Special Thanks:

- Jack Graziano - NASA DEVELOP Lead, Langley Research Center

6. Glossary

Agency for Toxic Substances and Disease Registry (ATSDR) – a branch of the CDC that determines the public health effects caused by environmental exposures.
Aerosol Optical Depth (AOD) – quantifies the optical thickness of aerosols, with higher values representing higher aerosol concentrations.
Centers for Disease Control and Prevention (CDC) – the federal science agency whose mission is to protect the public's health.
Climate Action Plan (CAP) – details the town of Davidson's climate adaptation and mitigation strategies and goals.
Comma-separated Value (CSV) – a file format that stores tabular data.
Earth Observations (EO) – satellites and sensors that provide data on Earth's biological, chemical, and physical systems

Ecosystem Spaceborne Thermal Radiometer Experiment on Space Station (ECOSTRESS) – a high-resolution sensor onboard the International Space Station used to capture a wide range of the electromagnetic spectrum.
Evapotranspiration (ET) – a measurement of how efficiently water leaves the Earth's surface and is absorbed by vegetation.
Geospatial Research, Analysis, and Services Program (GRASP) – a CDC and ATSDR program that releases geospatial data from these agencies.
Heat Hot Spot (HHS) – an area of increased temperature, usually due to urbanization, lack of healthy vegetation, or high amount of exposed, impervious surfaces.
Land surface temperature (LST) – the temperature on the surface of the Earth.
National Agriculture Imagery Program (NAIP) – a program that captures and publishes aerial imagery of the Earth.
Normalized difference vegetation index (NDVI) – a metric that quantifies density and health of vegetation. On a scale between –1 to 1, a higher value represents denser and healthier vegetation.
Operational land imager (OLI) – a sensor on Landsat 8 and 9 that measures the visible, near infrared, and short-wave infrared portions of the spectrum. Provides sufficient resolution to distinguish between urban centers, farms, forests, and other land uses.
Social Vulnerability Index (SVI) – an evaluation of socioeconomic and demographic factors that affect populations' vulnerabilities.
Thermal infrared sensors (TIRS) – on Landsat 8 and 9 to measure land surface temperature using two thermal infrared bands.
Urban Heat Island (UHI) – pockets of urban areas that are warmer than surrounding rural areas due to reduced vegetation and increased human activities.
United States Geological Survey (USGS) – the federal scientific agency largely responsible for releasing Earth, water, biological, and mapping data.

7. References

Andres-Anaya, P., Sanchez-Aparicio, M., Del Pozo, S., Lagüela, S., Hernández-López, D., & Gonzalez-Aguilera, D. (2023). A new methodology for estimating surface albedo in heterogeneous areas from satellite imagery. *Applied Sciences, 14*(1), 75. https://doi.org/10.3390/app14010075

Centers for Disease Control and Prevention, & Agency for Toxic Substances and Disease Registry. (2024, December 16). *SVI data & documentation download.* [Data set]. Geospatial Research, Analysis, and Services Program. https://www.atsdr.cdc.gov/place-health/php/svi/svi-data-documentation-download.html

Cheela, V., John, M., Biswas, W., & Sarker, P. (2021). Combating urban heat island effect—a review of reflective pavements and tree shading strategies. *Buildings*, *11*(3), 93. https://doi.org/10.3390/buildings11030093

Chen, X.L., Zhao, H.M., Li, P.X., & Yin, Z.Y. (2006). Remote sensing image-based analysis of the relationship between urban heat island and land use/cover changes. *Remote Sensing of Environment*, *104*(2), 133–146. https://doi.org/10.1016/j.rse.2005.11.016

D'Allestro, P., & Parente, C. (2015). GIS application for NDVI calculation using Landsat 8 OLI images. *International Journal of Applied Engineering Research*, *10*(21), 42099–42102.

Davidson Lands Conservancy. *Treesdavidson.* Retrieved August 4, 2025, from https://davidsonlands.org/explore-nature/trees-davidson/

Earth Resources Observation and Science (EROS) Center. (2020). Landsat 8-9 Operational Land Imager / Thermal Infrared Sensor Level-2, Collection 2 [Data set]. U.S. Geological Survey. Retrieved July 7, 2025, from https://doi.org/10.5066/P9OGBGM6

Hook, S., Fisher, J. (2019). ECOSTRESS Evapotranspiration PT-JPL Daily L3 Global 70 m V001 [Data set]. NASA EOSDIS Land Processes Distributed Active Archive Center. Retrieved July 16, 2025, from https://doi.org/10.5067/ECOSTRESS/ECO3ETPTJPL.001

Hook, S., & Hulley, G. (2019). *ECOSTRESS Land Surface Temperature and Emissivity Daily L2 Global 70 m V001* [Data set]. NASA Land Processes Distributed Active Archive Center. Retrieved July 16, 2025, from https://doi.org/10.5067/ECOSTRESS/ECO2LSTE.001

Hu, Y., Jia, G., Gao, H., Li, Y., Hou, M., Li, J., & Miao, C. (2023). Spatial characterization of global heat waves using satellite-based land surface temperature. *International Journal of Applied Earth Observation and Geoinformation*, *125*, 103604. https://doi.org/10.1016/j.jag.2023.103604

Loughner, C. P., Allen, D. J., Zhang, D.-L., Pickering, K. E., Dickerson, R. R., & Landry, L. (2012). Roles of urban tree canopy and buildings in urban heat island effects: Parameterization and preliminary results. *Journal of Applied Meteorology and Climatology*, *51*(10), 1775–1793. https://doi.org/10.1175/jamc-d-11-0228.1

MacroTrends. (2025). Charlotte Metro Area Population 1950-2025. https://www.macrotrends.net/global-metrics/cities/22954/charlotte/population

National Agriculture Imagery Program—NAIP hub site. Retrieved July 17, 2025, from https://naip-usdaonline.hub.arcgis.com/

Quantify interrater agreement with kappa. Retrieved July 17, 2025, from https://www.graphpad.com/quickcalcs/kappa1/

Town of Davidson. (2024). *Climate Action Plan*. Climate Action Plan | Davidson, NC – Official Website. https://www.townofdavidson.org/1508/Climate-Action-Plan

USGS (2023). How do I use a scale factor with Landsat Level-2 science products? https://www.usgs.gov/faqs/how-do-i-use-a-scale-factor-landsat-level-2-science-products

World Health Organization. (2024). *Heat and health*. https://www.who.int/news-room/fact-sheets/detail/climate-change-heat-and-health

Zargari, M., Mofidi, A., Entezari, A., & Baaghideh, M. (2024). Climatic comparison of surface urban heat island using satellite remote sensing in Tehran and Suburbs. *Scientific Reports*, *14*(1). https://doi.org/10.1038/s41598-023-50757-2

Zhao, Q., Guo, Y., Ye, T., Gasparrini, A., Tong, S., Overcenco, A., Urban, A., Schneider, A., Entezari, A., Vicedo-Cabrera, A. M., Zanobetti, A., Analitis, A., Zeka, A., Tobias, A., Nunes, B., Alahmad, B., Armstrong, B., Forsberg, B., Pan, S.-C., … Li, S. (2021). Global, regional, and national burden of mortality associated with non-optimal ambient temperatures from 2000 to 2019: A three-stage modelling study. *The Lancet Planetary Health*, *5*(7). https://doi.org/10.1016/s2542-5196(21)00081-4

8. Appendices

Appendix A: *Social Vulnerability Index*

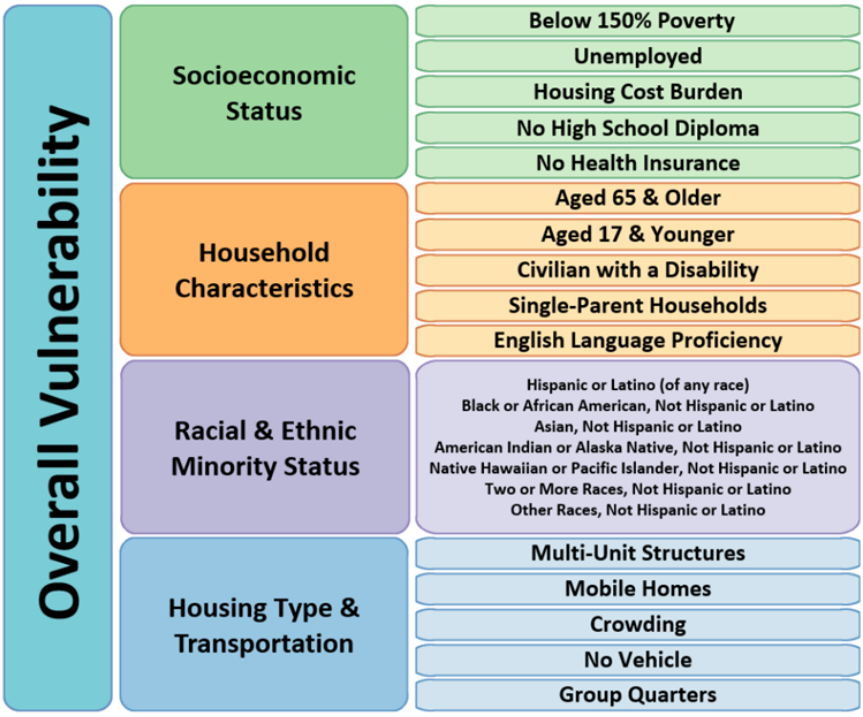

Figure A1. The CDC / ATSDR Social Vulnerability Variables

Table A1
Selected SVI Variables

Variable	Vulnerability Theme
Percentage of persons below 150% poverty estimate	Socioeconomic status
Unemployment rate estimate	Socioeconomic status
Percentage of housing cost-burdened occupied housing units with annual income less than $75,000 (30%+ of income spent on housing costs) estimate, 2018-2022 ACS estimate, 2018-2022 ACS	Socioeconomic status
Percentage of persons with no high school diploma (age 25+) estimate	Socioeconomic status
Percentage uninsured in the total civilian noninstitutionalized population estimate, 2018-2022 ACS	Socioeconomic status
Percentage of persons aged 65 and older estimate, 2018-2022 ACS	Household characteristics
Percentage of civilian noninstitutionalized population with a disability estimate, 2018- 2022 ACS	Household characteristics
Percentage of single-parent households with children under 18 estimate, 2018-2022 ACS	Household characteristics
Percentage of persons (age 5+) who speak English "less than well" estimate, 2018-2022 ACS	Household characteristics
Percentage of housing in structures with 10 or more units estimate	Housing type & transportation
Percentage of mobile homes estimate	Housing type & transportation
Percentage of occupied housing units with more people than rooms estimate	Housing type & transportation
Percentage of households with no vehicle available estimate	Housing type & transportation

Appendix B*: Earth Observations*

Table B1
Datasets used in this study

Dataset	Spatial Resolution	Time Period	Description	Source
Landsat 8 OLI	30m	2015-2025	Red and Near-Infrared Bands used to calculate NDVI; surface reflectance used to calculate albedo	USGS Earth Explorer
Landsat 8 TIRS	100m	2015-2025	Band 10 (long-wave infrared) used to calculate LST	USGS Earth Explorer
Landsat 9 OLI-2	30m	2021-2025	Red and Near-Infrared Bands used to calculate NDVI; surface reflectance used to calculate albedo	USGS Earth Explorer
Landsat 9 TIRS-2	100m	2021-2025	Band 10 (long-wave infrared) used to calculate LST	USGS Earth Explorer
ECOSTRESS	70m	2018-2025	Evapotranspiration and Nighttime LST	NASA Earthdata Search
NAIP	1m (2016), 0.6m (2022)	2016-2022	High-resolution aerial imagery used for tree canopy classification	USGS Earth Explorer
SVI	N/A	2022	Evaluation of socioeconomic factors to assess vulnerability	CDC & ATSDR

Appendix C: *Seasonal Distribution of Images Used*

Table C1

Seasonal Distribution of Landsat Images

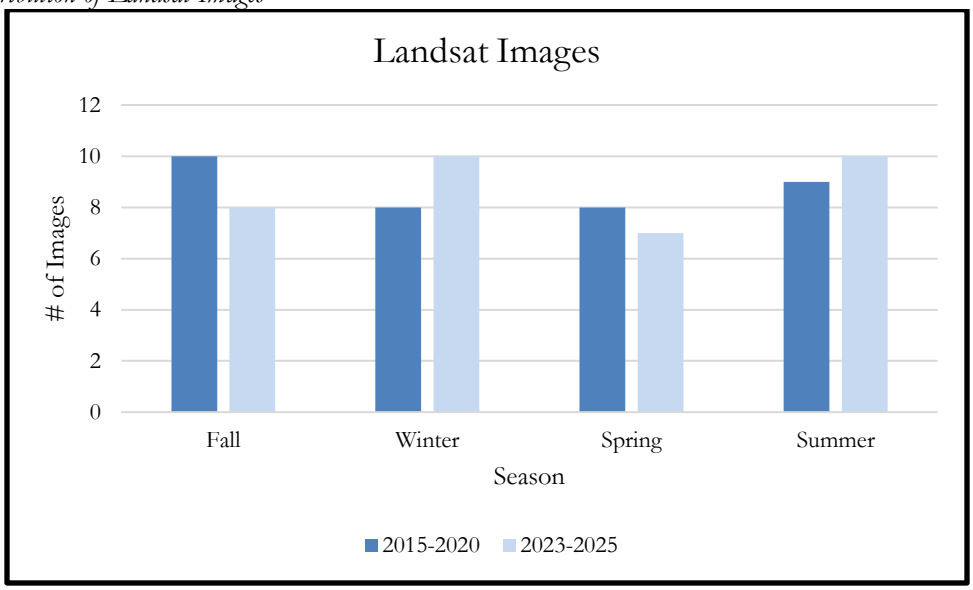

Table C2

Seasonal Distribution of ECOSTRESS nighttime LST Images

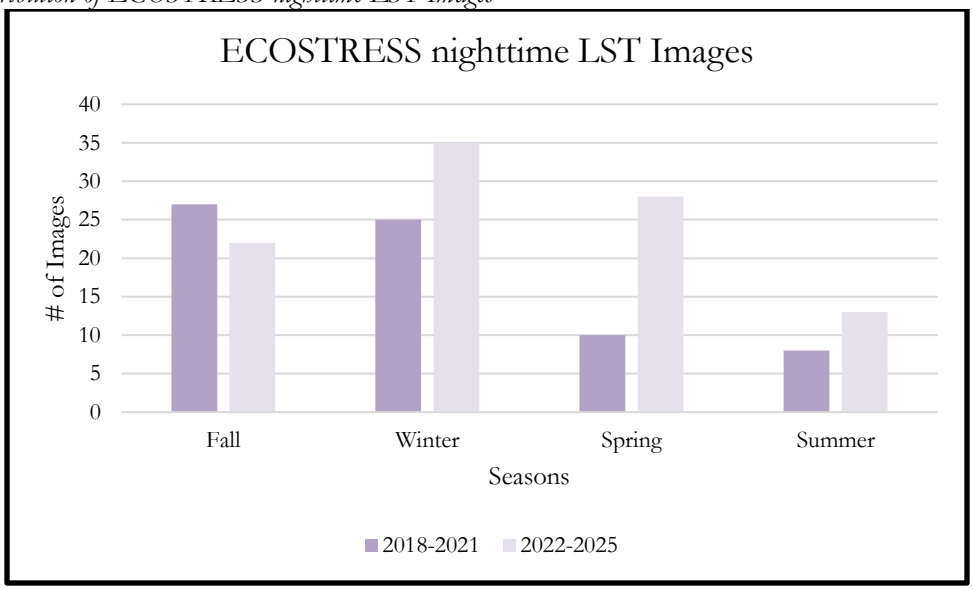

Table C3

Seasonal Distribution of ECOSTRESS Evapotranspiration Images

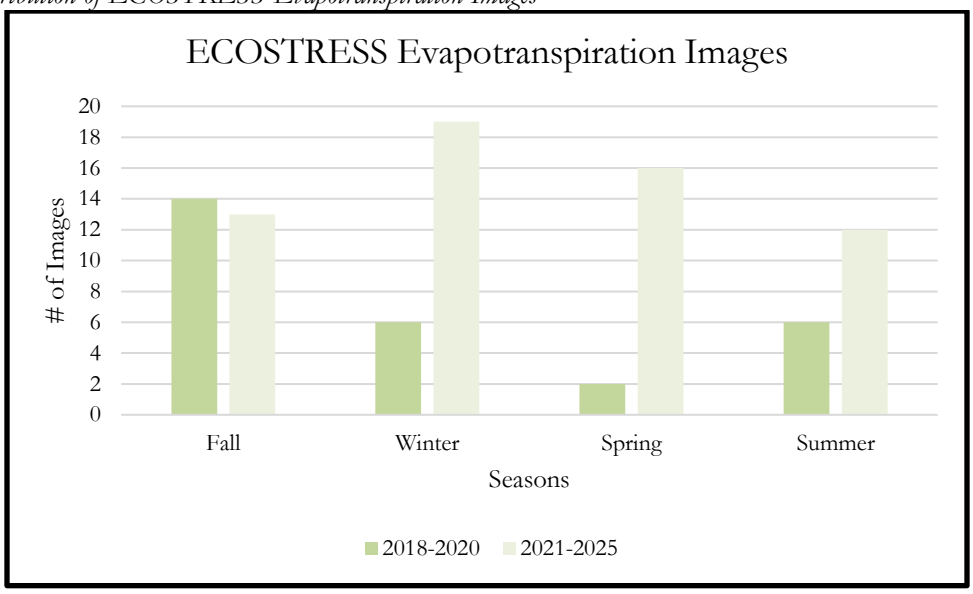

Appendix D: *Result Maps*

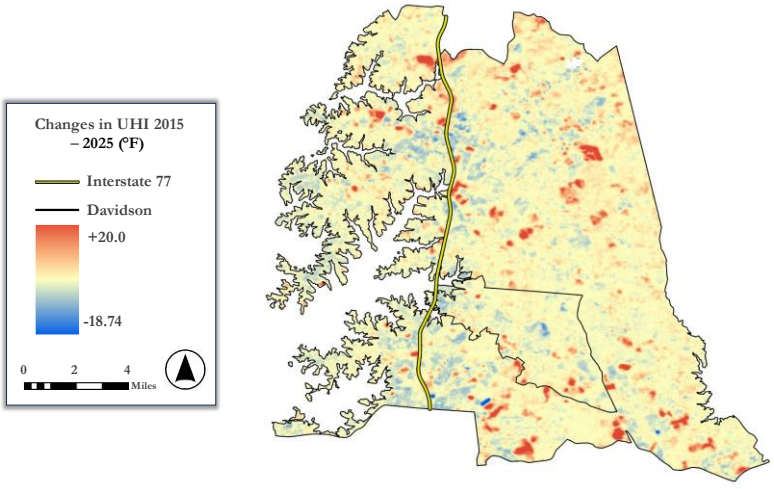

Figure D1. Changes in UHI, 2015-2020 through 2023-2025

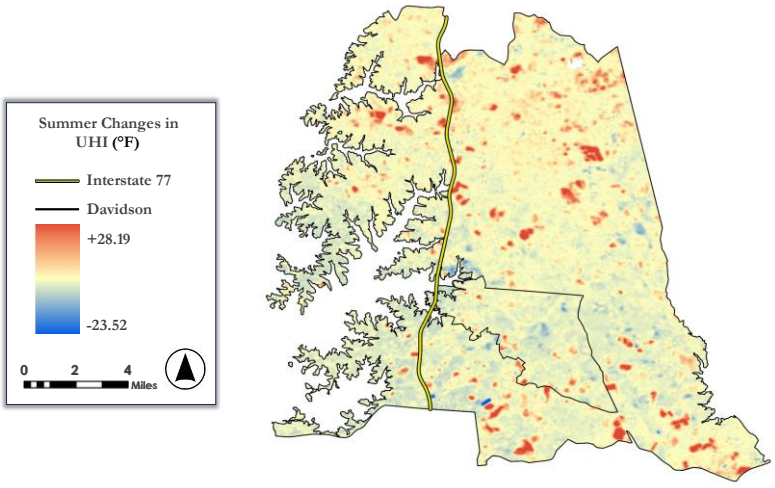

Figure D2. Summer changes in UHI, 2015-2020 through 2023-2025

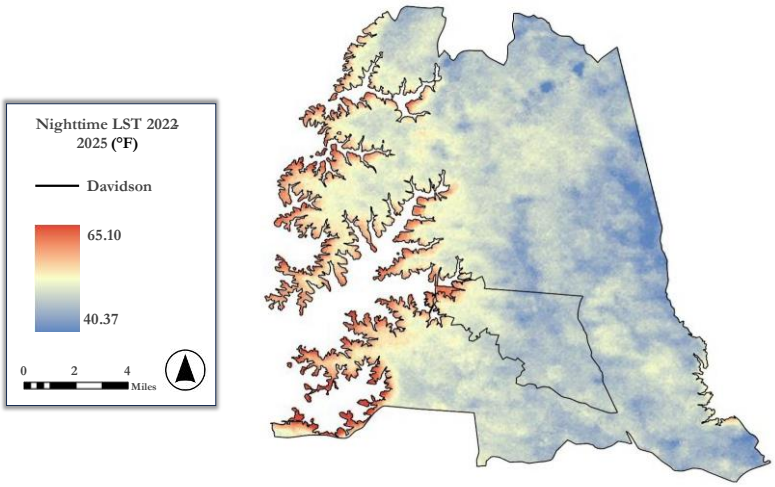

Figure D3. Nighttime LST, 2022-2025

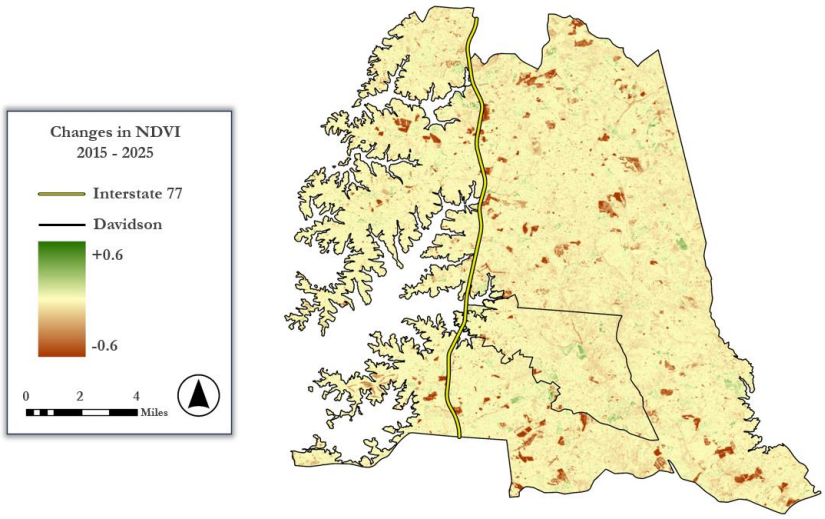

Figure D4. Changes in NDVI, 2015-2020 through 2023-2025

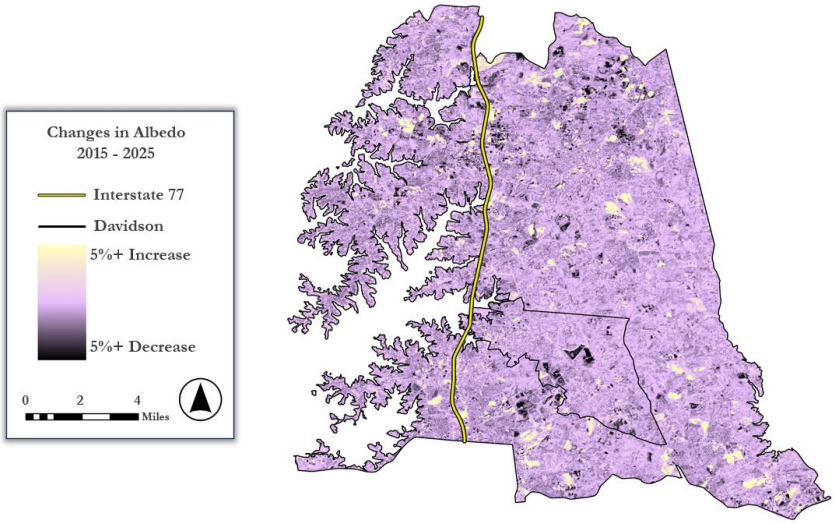

Figure D5. Changes in albedo, 2015-2020 through 2023-2025

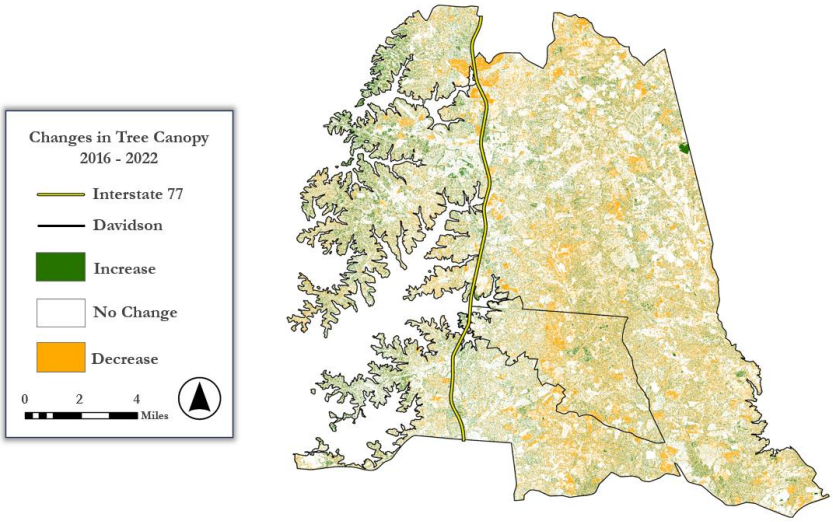

Figure D6. Changes in Tree Canopy, 2016-2022

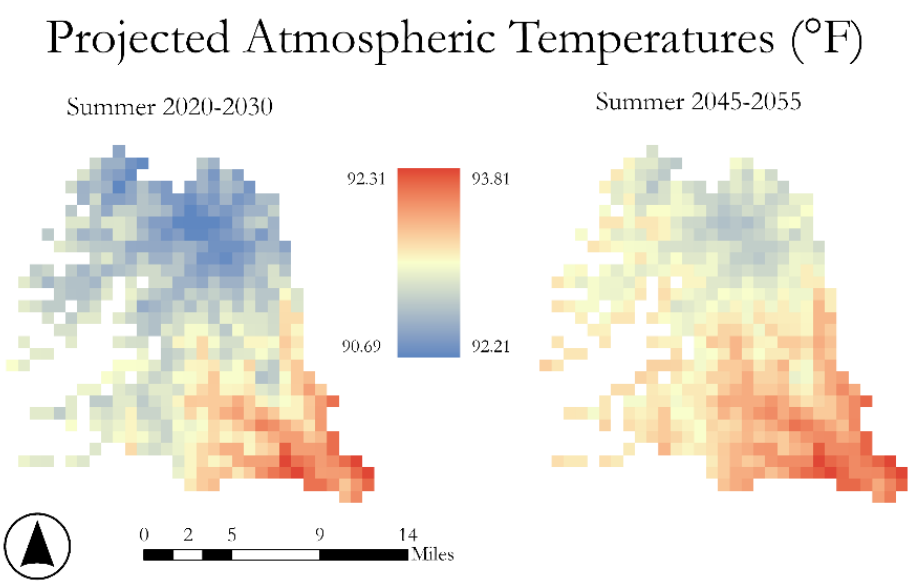

Figure D7. Projected Atmospheric Temperatures

Appendix E: *Supplemental Maps*

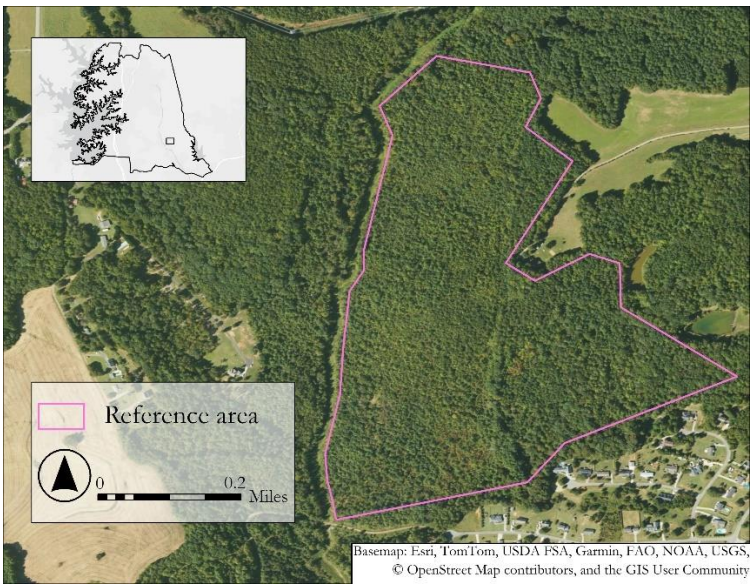

Figure E1: Vegetated Reference Area

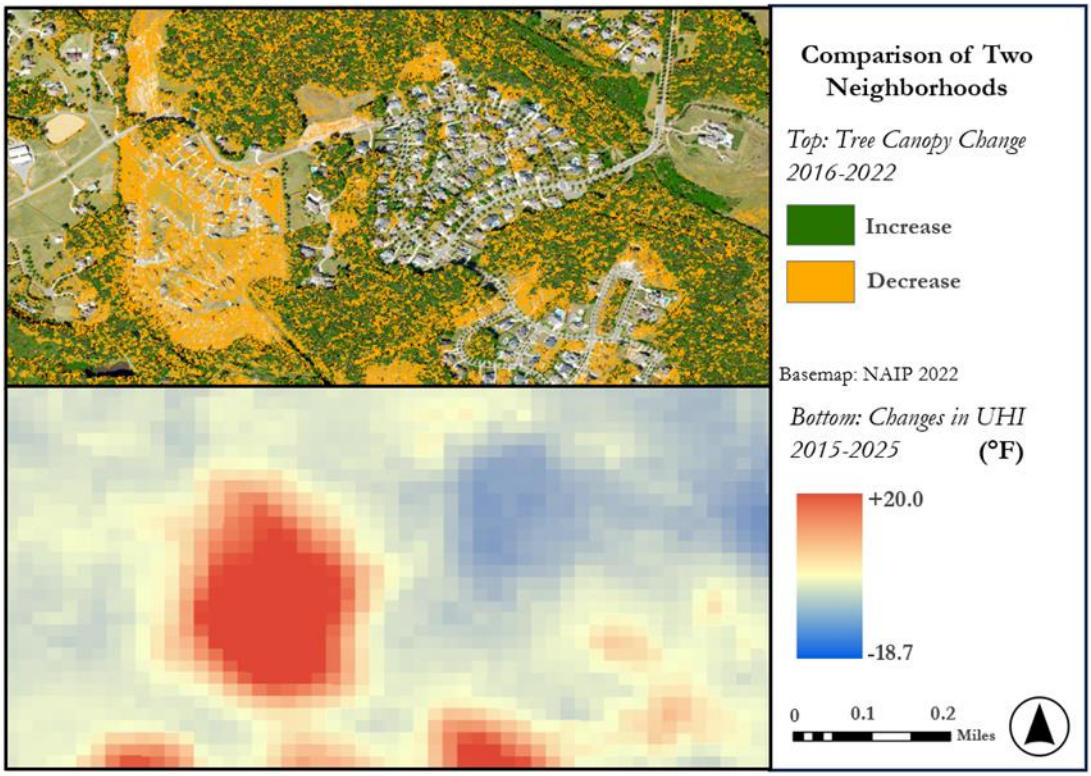

Figure E2. Zoom-in Observation of Tree Canopy and UHI

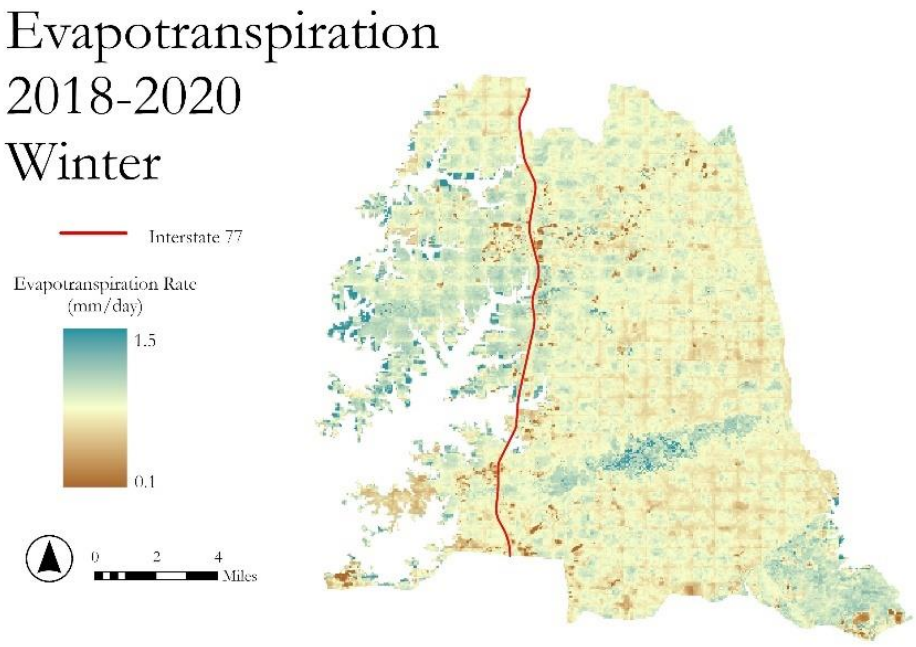

Figure E4. Evapotranspiration, Winter 2018-2020

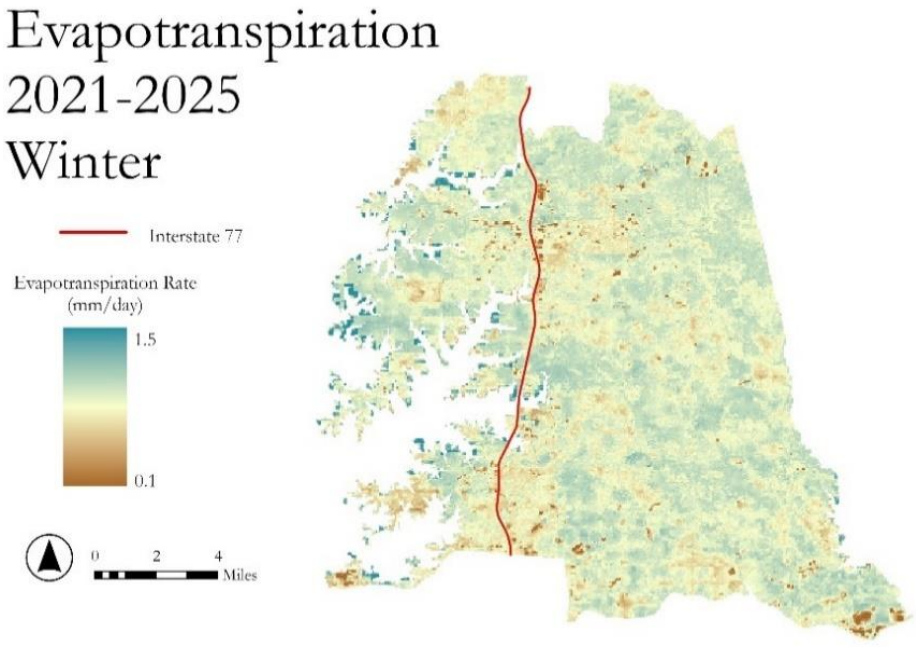

Figure E5. Evapotranspiration, Winter 2021-2025

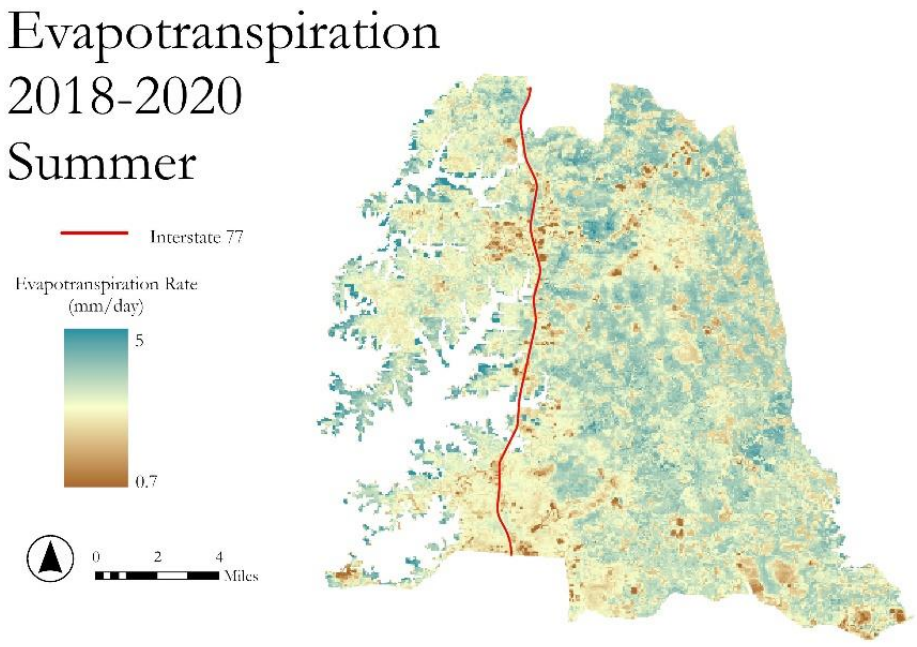

Figure E6. Evapotranspiration, Summer 2018-2020

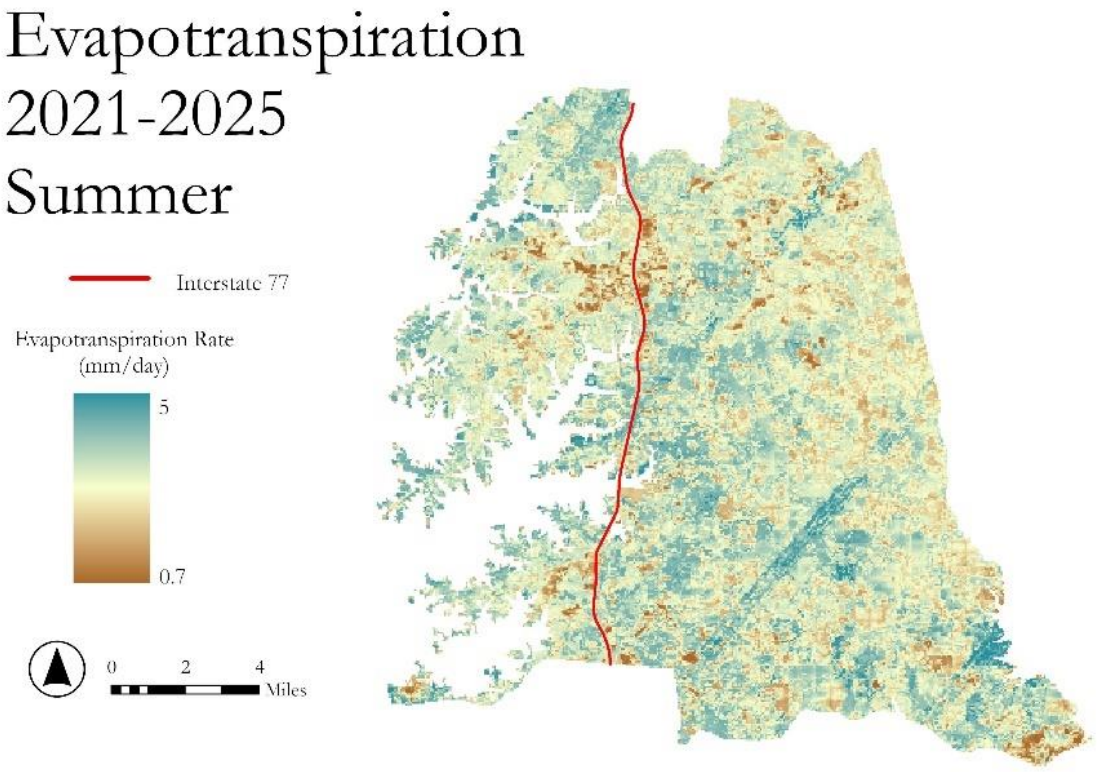

Figure E7. Evapotranspiration, Summer 2021-2025

Appendix F: *Supplemental Figures*

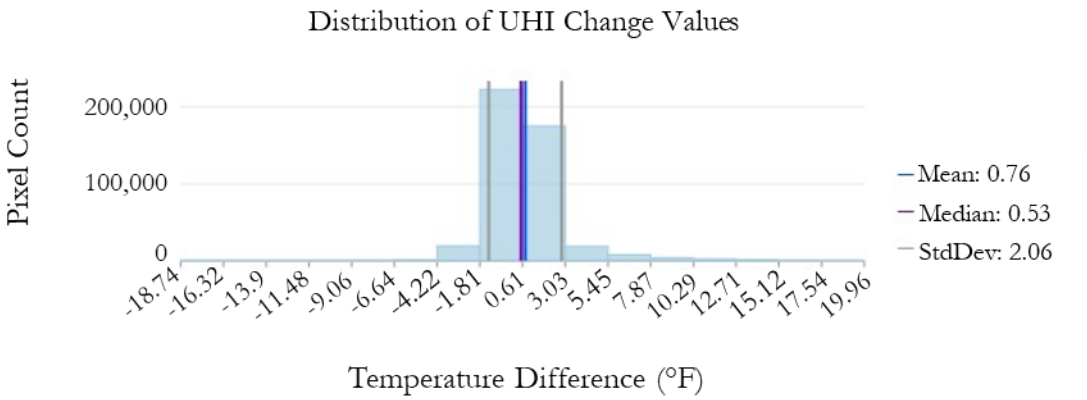

Figure F1. *Distribution of UHI Change Values*

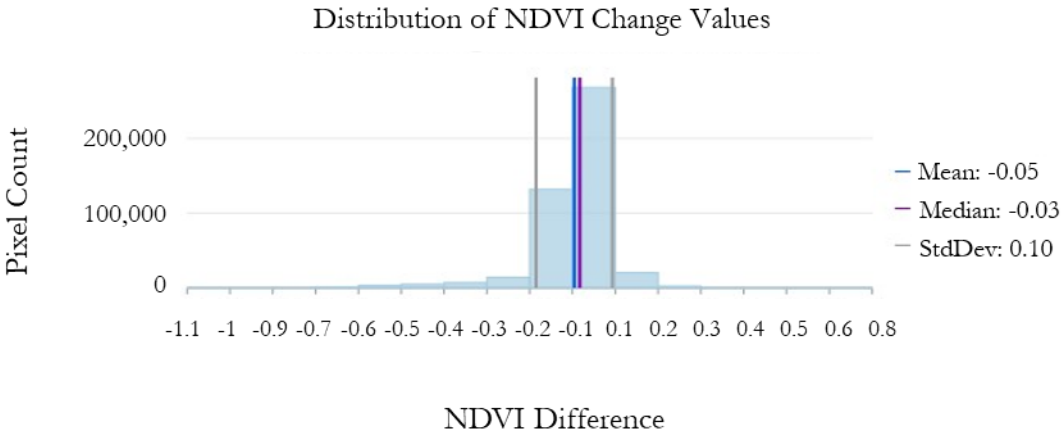

Figure F2. *Distribution of NDVI Change Values*

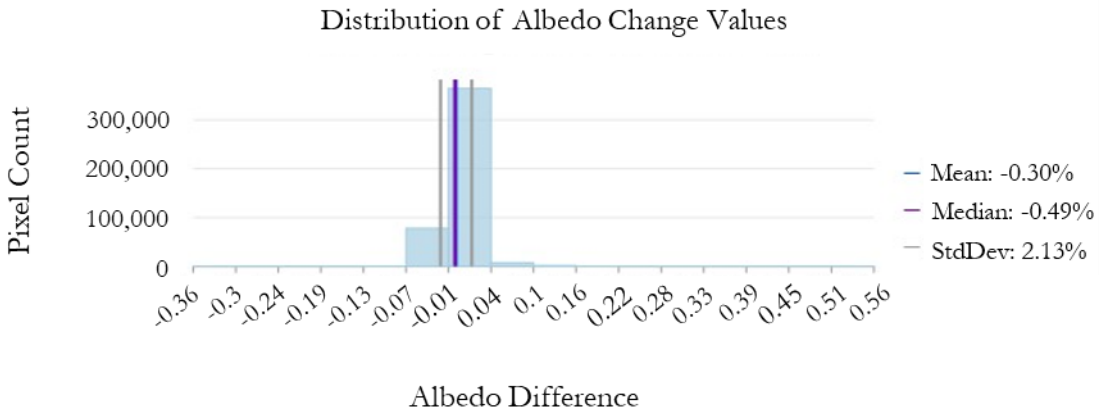

Figure F3. *Distribution of Albedo Change Values*

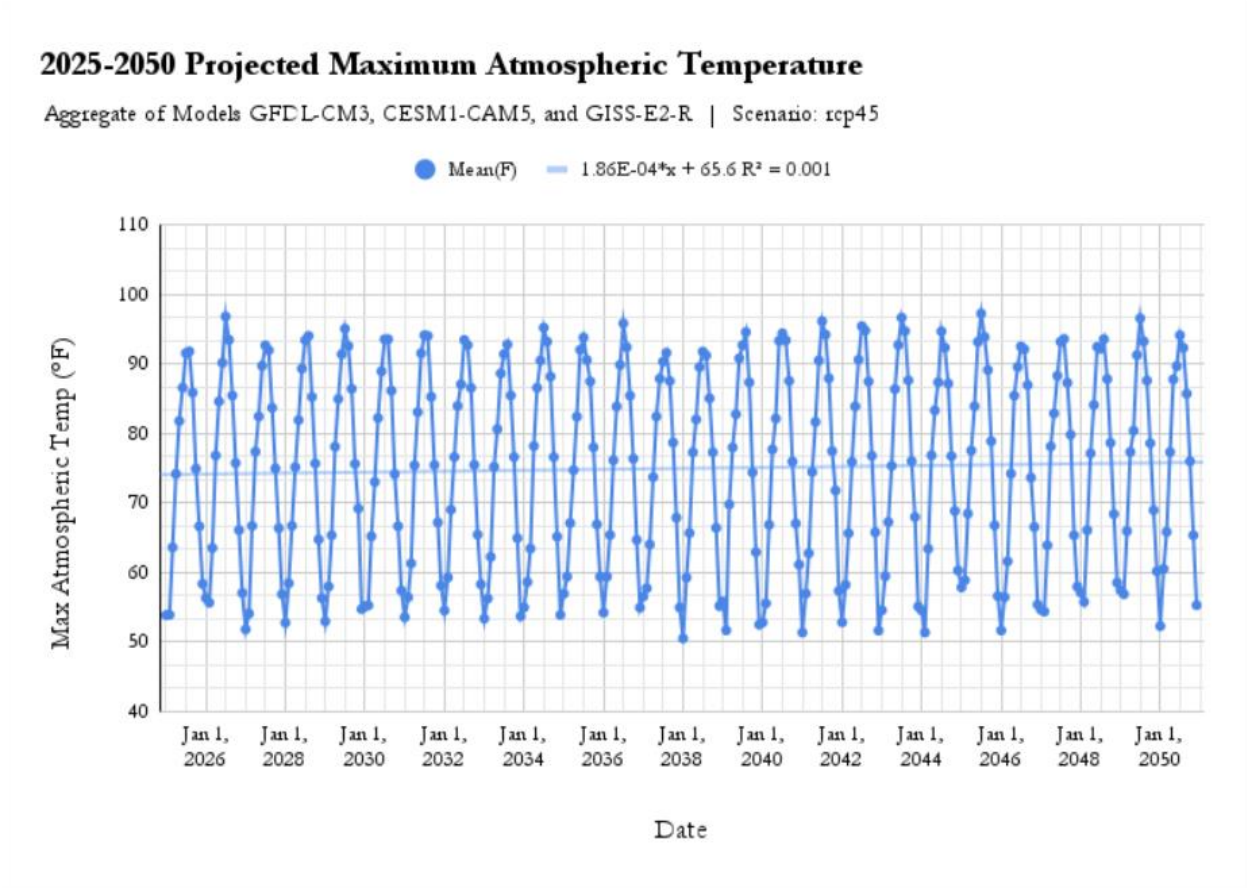

Figure F4. Projected Atmospheric Temperature Time Series, 2025-2050